Surface sensitivity of four-probe STM for the measurement of the resistivity of bulk ZnO correlated to XPS

Alex M. Lord[1*β], Jon E. Evans[1β], Chris J. Barnett[2β], Martin W. Allen[3β], Andrew R. Barron[2,4], Steve P. Wilks[5]

[1] Centre for NanoHealth, College of Engineering, University of Swansea, Singleton Park, SA2 8PP, United Kingdom.

[2]Energy Safety Research Institute (ESRI), College of Engineering, Swansea University Bay Campus, Fabian Way, Swansea, SA1 8EN, Wales, UK

[3]MacDiarmid Institute for Advanced Materials and Nanotechnology, Department of Electrical and Computer Engineering, University of Canterbury, Private Bag 4800, Christchurch, 8014, New Zealand

[4]Department of Materials Science and Nanoengineering, Rice University, 6100 Main MS-325, Houston, TX 77005, USA

[5]Multidisciplinary Nanotechnology Centre, Department of Physics, College of Science, University of Swansea, Singleton Park, SA2 8PP, United Kingdom.

*Corresponding Author: a.m.lord@swansea.ac.uk

β – authors contributed equally to the work

Abstract

Multi-probe instruments based on scanning tunnelling microscopy (STM) are becoming increasingly common for their ability to perform nano- to atomic-scale investigations of nanostructures, surfaces and *in situ* reactions. A common configuration is the four-probe STM often coupled with *in situ* scanning electron microscopy (SEM) that allows precise positioning of the probes onto surfaces and nanostructures enabling electrical and scanning experiments to be performed on highly localised regions of the sample. In this paper, we assess the sensitivity of four-probe STM for in-line resistivity measurements of the bulk ZnO surface. The measurements allow comparisons to established models that are used to relate light plasma treatments (O and H) of the surfaces to the resistivity measurements. The

results are correlated to x-ray photoelectron spectroscopy (XPS) and show that four-probe STM can detect changes in surface and bulk conduction mechanisms that are beyond conventional monochromatic XPS.

Introduction

The four-probe scanning tunnelling microscopy (4p-STM) technique combined with *in situ* scanning electron microscopy (SEM) was pioneered by Hasegawa and co-workers beginning in 2000 and the proceeding years after.[1–3] Since that era the technique has been commercialised and combined with numerous other *in situ* capabilities to achieve some incredible results on various surfaces and nanomaterials. Some notable results have refined our knowledge of defects in topological insulators using scanning tunnelling potentiometry,[4] contacting and manipulating single atoms at 4K,[5] tuning of atomic chains by chemisorption,[6] conductance measurements of self-assembled single layer molecules,[7] identification of metallic twin grain boundaries on monolayers,[8] charge transport in nanowires,[9–13] and using four-probe measurements to separate surface and atomic step conductivity from bulk conductivity.[14,15]

In the area of sensors, where surface modification is typically used to induce a change in the electrical conductivity of a device, for example via adsorption,[16] covalent attachment or bio-functionalisation[17], understanding the details of surface modification and correlating these details with the changes in surface conductivity due to band bending and the influence of surface states is a crucial step in realising the potential of such devices. These devices depend on changes in channel conductivity, typically this necessitates that one of the dimensions of the channel is reduced to the nanoscale at which the Debye length becomes a significant fraction of the relevant dimension. This is now commonly achieved by incorporating semiconductor nanostructures such as nanowires, nanosheets and more exotic structures into these devices.

However, when studying surface modification, there exist challenges in applying standard surface science methods to nanostructures such as free standing nanowires, likely due to the complications encountered when dealing with samples varying significantly from the semi-infinite 2D sheets best suited for relatively large area surface averaging techniques such as XPS, FTIR, Raman and ellipsometry.[18] Electrical conductivity measurements of

nanostructures which are inherently surface sensitive have become routine using lithography and multiprobe STM; however, studies of surface modification using established techniques are complicated by the morphology and dimensions of the nanostructures. Conversely, large area surface science techniques have matured around the study of semiconductor single crystals but true surface sensitive conductivity measurements on bulk substrates using micro four point probe remain rare.

For an idealised collinear four point probe measurement, the measured bulk resistance is inversely proportional to the contact spacing, whereas the surface resistance is independent of contact spacing.[19] Therefore, local surface sensitive conductivity measurements can be made on macroscale semiconductor single crystals provided the current probe contact spacing is made sufficiently small. Accurate sub-micron positioning of sharp probes made possible by multi-probe STM/SEM allow flexible surface sensitive conductivity measurements to be made without the need for advanced and permanent lithographic processing or the fabrication of monolithic microscale four-point probe devices.

Here we present four-point probe surface sensitive conductivity measurements conducted on a ZnO single crystal modified via simple surface plasma treatments. The four-point probe conductivity measurements are compared with valence-band and core-level XPS in order to validate the effects of these treatments on surface conduction.

The results show that correlation of surface modifications on relatively well understood, highly ordered and readily characterisable single crystal substrates with surface sensitive electrical conductivity measurements are possible. In addition, the multi-probe technique is shown to provide invaluable insight's when studying changes in surface electrical conductivity that are relevant when device dimensions are reduced down towards the nanoscale.

Zinc Oxide (ZnO) is a metal oxide semiconductor with a wide band gap on 3.37 eV and high exciton binding energy of 60 meV.[20] Over recent years it has attracted a significant amount of scientific research due to its properties that include high transparency, piezoelectricity, high electron mobility and room temperature ferromagnetism.[21] ZnO can be formed into large single crystals as well as a number of nanostructures including nanowires, nanorods and nanosheets.[22,23]

ZnO crystallizes into the wurtzite structure which when viewed along the c-axis consists of alternating planes of Zn and O atoms, arranged in threefold coordinated "double layers" separated by a single Zn–O bond. Truncation of the crystal along this axis always results in one of two polar surfaces—the Zn-polar (0001) Zn-face or the O-polar ZnO ($000\bar{1}$) O-face. Due to the large electronegativity of oxygen, these polar faces have a significant ionic character and are electrostatically unstable.[24,25] Three stabilization mechanisms are commonly proposed: (a) a fractional negative charge transfer from the O-polar to Zn-polar face; (b) a surface reconstruction which removes 25% of the surface atoms; (c) the adsorption of hydroxide (hydrogen) on the Zn-polar (O-polar) face.[24–27] In the case of the Zn-polar face, some form of condition-dependent (i.e., pH, temperature, H_2/ H_2O partial pressure) competition between the formation of triangular islands and pits with O-terminated step edges and the adsorption of hydroxyl (OH) groups may occur.[26,27] The O-polar face, except under rare circumstances, has been shown to exhibit an unreconstructed 1x1 H-termination and was therefore chosen for this study to simplify the interpretation of the electrical and XPS measurements.[28,29]

Methods

Sample preparation

ZnO single crystal grown by SurfaceNet Gmbh was cut and polished normal to the *c*-axis such that the ($000\bar{1}$) facet was uppermost on which the measurements were performed. The same wafer was cleaved into portions such that the same crystal could be used for the several treatments and measurements that were performed. Measurements were attempted on the sample fresh from the packaging but contamination prevented conductive electrical contacts to be achieved. Therefore, the as-received samples discussed in the manuscript were treated with a standard solvent clean of ultrasonically agitated acetone, methanol and IPA.

Short plasma treatments using oxygen or hydrogen gases were applied using an SPTS inductively coupled plasma system for duration of 5 minutes. A short exposure was chosen to limit the effect to the surface and not induce any sub-surface modifications such as defects or doping that longer, e.g. 1 hour, plasma treatments create.[30,31] Gases were introduced to the chamber at a flow rate of 100 sccm and a chamber pressure of 20 mTorr

was maintained throughout the treatment. A power of 400 W was supplied by the RF generator to the chamber coil, with the platen generator switched off so as not to bias the sample.

Multi-probe STM electrical measurements

The single crystal ZnO samples were mechanically fixed to the sample plates and loaded into the UHV chamber (base pressure $1x10^{-11}$ mbar) and measurements were performed at least 24 hours after loading to eliminate the effect of residual photo-induced carriers. Nanoscale two-point and four-point probe measurements were carried out with an Omicron LT Nanoprobe with *in situ* SEM using a Keithley 2636B sourcemeter. Tungsten STM tips were etched in a solution of 2 Mol KOH using the method described by Ibe.[32] The tips were direct current annealed in UHV to remove probe oxide using the method described by Cobley *et al.*[33] to minimise the field effects caused by shank oxide.[34] The tips where approached with the automated tunnelling feedback function. Once the 1 nA setpoint was reached the tip was retracted and the feedback function was disengaged. The tips were then manually lowered in 1 nm steps until a current above the noise was observed on to the sample to avoid local modifications to the crystal surface that may affect the resistance measurements.[9,11,35–37]

For the two-point probe measurements the tips were lowered to the surface in this manner on to the sample surface and current-voltage (I-V) measurements were taken in the transmission line fashion. Four-point probe measurements were performed in a linear configuration with the outer probes supplying the current and the inner sense probes measuring the voltage drop. I-V measurements were taken with the outer probes at fixed separation and the inner probe separation was varied to investigate bulk resistivity. Additionally, measurements were performed with the inner probes at fixed separation and the outer probe separation varied to investigate the surface resistivity and sensitivity of the four-probe STM technique to probe configurations.[38,39]

X-ray photo-electron spectroscopy (XPS)

The samples were analysed using a Kratos Axis Ultra-DLD photoelectron spectrometer at the University of Auckland, New Zealand, utilising monochromatic Al Kα radiation (*hv* = 1486.6)

from a source operating at 150 *W* with an effective energy resolution of ~400 *meV*, and a take-off angle of 90°. Each sample was electrically grounded to the spectrometer to avoid sample charging and to enable the zero of the binding energy (BE) scale to be directly referenced to the Fermi level of each sample. In each case the analysis area was 700 µm by 300 µm. Survey spectra were collected at a pass energy of 160 *eV*, from -5 *eV* to 1300 *eV*, while high resolution spectra were collected between 526 *eV* and 538 *eV* (O 1s), from 1015 *eV* to 1030 *eV* (Zn 2p 3/2), from 280 *eV* to 295 *eV* (C 1s) and valence band (VB) spectra were collected over the range -4 *eV* to 15 *eV*. For each high resolution scan a pass energy of 20 *eV* was used.

Results and discussion

Four-probe STM was used to measure the resistivity of the three sample types: As-received (AR), hydrogen plasma treated and oxygen plasma treated. The probes were manually lowered to the surface with nanometre precision in 1 nm steps until a current above the noise level was observed. Two-probe I-V sweeps ($\pm$0.2V) were then performed between each of the probes to ensure the probe contacts were conductive and the I-V graphs were linear, a current of µA magnitude was typically recorded. It should be noted here that it was not possible to achieve conductive contacts to the sample with no cleaning treatment and as such the as-received sample underwent a standard solvent cleaning process.[40]

The four contacts were aligned in a straight line, known as an in-line measurement, as shown in Figure 1. Due to the highly conductive nature of the samples four probe sweeps were taken at $\pm$0.5 mV where a current of several µA's was recorded. The current was comparable to the two-probe I-V sweeps at $\pm$0.2 V which displays the inherent need to use the four probe configuration to overcome the contact resistance for accurate electrical resistivity measurements.[39]

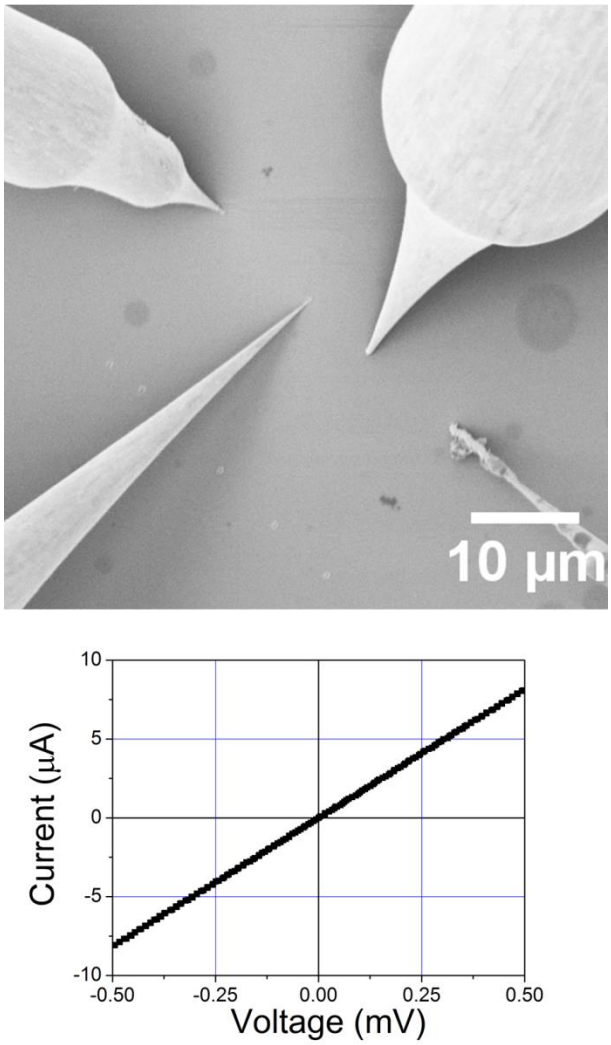

Figure 1. In situ SEM image from the four-probe STM instrument of a typical probe configuration used for the in-line resistivity measurements along with the four probe I-V measurement of a hydrogen plasma treated sample.

Native ZnO is well known to be n-type conductive and although the source of this intrinsic doping remains controversial, oxygen vacancies are thought to be deep donors (~0.8 to 1.0 eV below the conduction band minimum (CBM) in ZnO and therefore are not expected to provide a source of the intrinsic n-type conductivity of ZnO.[41,42] However, Janotti and Van de Walle showed in those works that multi-coordinated H trapped inside an oxygen vacancy is predicted to be a significant shallow donor. Oxygen plasma treatment may displace hydrogen from oxygen vacancies by the filling/annihilation of oxygen vacancies. Furthermore, Brillson et al. have shown that the density of oxygen vacancies can significantly increase in the near-surface region.[43] Hydrogen is well characterised as an electron donor in ZnO, with previous studies suggesting that the presence of hydrogen in

the form of hydroxyl termination of the bulk lattice results in a surface electron accumulation layer (downward band bending) for bulk single crystals.[44,45]

For micro four-point probe measurements (4pp) on a bulk substrate with the probes far away from any boundaries the sample may be approximated by a semi-infinite volume of uniform resistivity material. The floating potential V_f in the material at a distance r from a point contact current probe is given by [14]:

$$V_f = \frac{\rho I}{2\pi r} \qquad \text{- Equation 1}$$

where ρ is the resistivity of the material. With two current probes in contact with the sample, each probe carries the same current magnitude but in opposite directions. The floating potential is then given by the difference in potentials induced by each of the current probes:

$$V_f = \frac{\rho I}{2\pi}\left(\frac{1}{r_1} - \frac{1}{r_4}\right) \qquad \text{- Equation 2}$$

where r_1 and r_4 are the distances from probes 1 and 4, respectively. If r_{21}, for example, represents the distance between probes 2 and 1, the floating potentials at voltage probes V_{f2} and V_{f3} may be written as:

$$V_{f2} = \frac{\rho I}{2\pi}\left(\frac{1}{r_{21}} - \frac{1}{r_{24}}\right) \quad \text{- Equation 3}$$

$$V_{f3} = \frac{\rho I}{2\pi}\left(\frac{1}{r_{31}} - \frac{1}{r_{34}}\right) \quad \text{- Equation 4}$$

The potential difference between the voltage probes is then:

$$V = V_{f2} - V_{f3} = \frac{\rho I}{2\pi}\left(\frac{1}{r_{21}} + \frac{1}{r_{34}} - \frac{1}{r_{24}} - \frac{1}{r_{31}}\right) \quad \text{- Equation 5}$$

In the case of the equidistant collinear four point probe configuration, this equation simplifies to:

$$V = \frac{\rho I}{2\pi r} \qquad \text{- Equation 6}$$

The four point probe resistance is defined to be:

$$R_{4pp} \equiv \frac{V}{I} \qquad \text{- Equation 7}$$

The resistivity of the material is then given by:

$$\rho = R_{4pp}\left(\frac{2\pi}{\frac{1}{r_{21}}+\frac{1}{r_{34}}-\frac{1}{r_{24}}-\frac{1}{r_{31}}}\right) \quad \text{- Equation 8}$$

where R_{4pp} is obtained from a linear fit to the four point measurement I-V characteristics.

Figure 2a shows resistivity values calculated using equation 8 (subsequently referred to as the apparent resistivity) plotted as a function of voltage (inner) probe separation with the current (outer) probes kept fixed at a separation of approximately 60 µm. A distinct change in apparent resistivity is seen following both plasma treatments. The as-received sample shows an apparent resistivity of ~0.45 Ωcm across the voltage probe separation range which is increased to ~0.6 Ωcm following oxygen plasma treatment and decreased to ~0.2 Ωcm following hydrogen plasma treatment.

In the case of a bulk homogeneous and semi-infinite sample this apparent resistivity should be independent of probe spacing. Here, where a plasma treatment has been applied, local changes in resistivity would be expected to be spatially confined to the surface, invalidating the assumption of homogeneity inherent in equation 8 and resulting in a dependence of apparent resistivity on probe separation. In figure 2a, a slight decrease in apparent resistivity is seen with reduced voltage probe spacing for all samples. This could be explained by the presence of downward band bending from a high conductivity electron accumulation layer at the surface of the as-received sample. Bands would then be modified either towards the flat band condition by oxygen plasma or further towards additional electron accumulation by the hydrogen plasma.

For reduced voltage probe separations on a bulk substrate in surface accumulation with a constant current being supplied by the outer probes, the measured voltage drop between the inner probes though the conductive surface will be less than expected for a bulk sample of uniform resistivity. This will lead to a lower 4pp resistance (equation 7), which when multiplied by the bracketed geometric correction factors in equation 8 will result in a decrease in apparent resistivity with voltage probe separation rather than the constant

resistivity expected from a homogenous semi-infinite sample. Larger surface electron accumulation will lead to a lower apparent resistivity and consequently a greater degree of dependence on voltage probe separation. This is what is observed for the three samples, with the lower apparent resistivity hydrogen treated sample exhibiting a higher dependence on voltage probe spacing.

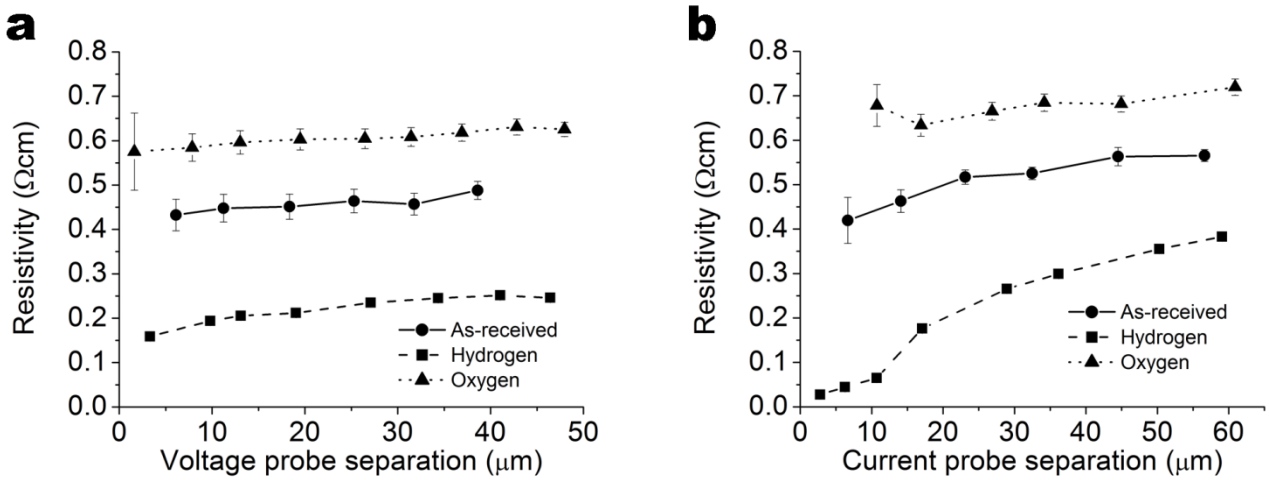

Figure 2. Four point probe resistivity calculated using the semi-infinite volume approximation (equation 8) showing resistivity as a function of (a) voltage probe separation keeping current probe separation constant and (b) current probe separation keeping voltage probe separation constant. The graphs include resistivity error bars for the H-treated sample but the deviation in values is such that they are not apparent.

To investigate this further, the inner voltage probes were kept fixed at a separation of <10 μm while the outer current probes were moved. As the current probe separation is reduced, for a homogeneous sample this has the effect of confining the current to the sample surface. If this assumption of homogeneity is invalid and surface conductivity is different to the bulk, this will be reflected in the apparent resistivity calculated using equation 8. Particularly for the hydrogen plasma treated sample, reducing the current probe separation results in a decrease in apparent resistivity from ~0.35 Ωcm at 60 μm probe separation to ~0.2 Ωcm at ~18 μm before a dramatic reduction is observed to <0.05 Ωcm below 10 μm probe separation, indicating the conductivity is higher at the surface for this treatment than in the bulk, which can be explained by the effect of H-plasma treatment loading oxygen vacancies with H (figure 2b). A similar trend for the as-received sample is also observed but with a much smaller change from ~0.5 Ωcm at 60 μm to ~0.4 Ωcm at 5 μm probe separation. The oxygen plasma treated sample shows much higher apparent resistivity as

expected for this treatment of ZnO and remains approximately constant at ~0.65 Ωcm indicating more insulating surface properties.[30] These trends of decreasing apparent resistivity with reduced current probe spacing are an expected consequence of a surface layer with higher conductivity than in the bulk. An apparent resistivity independent of probe spacing would indicate a homogenous sample i.e. flat band conditions at the surface. The fact that all samples exhibit this downward trend suggests some degree of surface electron accumulation is present in all samples. For the as-received and hydrogen treated samples shown in Figure 2b, it is clear that surface conduction is prominent which has been previously observed by Allen et al.[40] amongst others,[46] even at the largest current probe separation of ~60µm (Figure 2b) due to the slight difference in resistivity between samples at this spacing when compared to the 40 µm and 50 µm measurements in Figure 2a, respectively .

Coppa et al. have used oxygen/helium plasma at elevated temperatures to clean $000\bar{1}$ single crystal zinc oxide and found that it improved the gold Schottky contacts, in a similar fashion to the use of pure oxygen plasma shown by Brillson et al.[30,47] Hydrogen plasma can be used to increase the carrier concentration of ZnO single crystal by up to an order of magnitude[48] and it has been seen that hydrogenation using H plasma can reduce the defect band measured using cathodoluminescence.[49] The short plasma treatments used here are thought to have minimal effect on the sub-surface defects that are usually modified by prolonged and aggressive plasma treatments.[30]

Core-level and Valence Band XPS

The effect of the surface treatments was investigated with core-level and valence band XPS. This is a useful tool for measuring near surface band bending and chemical modifications and has been widely applied for the investigation of the bulk ZnO surface and many of the facets.[44,50–52]

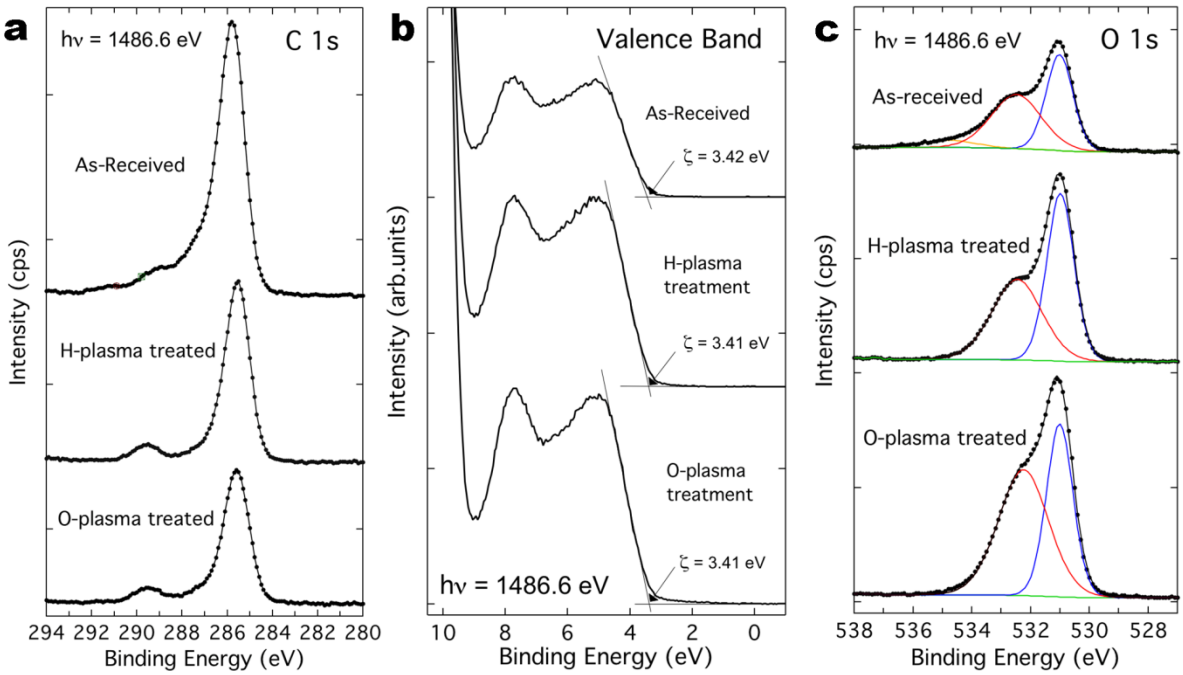

Figure 3. XPS data for the as-received sample, the hydrogen plasma treated sample and the oxygen plasma treated samples: a) the carbon C 1s peak; b) the valence band edge showing minimal change in ζ the valence band edge for the three samples; c) the oxygen O 1s peak and surface-associated secondary peak displaying a significant difference on the oxygen plasma treated sample.

Figure 3a shows the C 1s peak for each of the samples and reduces significantly for the plasma treated samples. This can be seen quantitatively in Table 1 that shows a reduction of 29.4% and 39.7% in surface associated carbon for the hydrogen and oxygen plasma treated samples, respectively. No significant change in the Zn 2p 3/2 peak was observed other than the Zn concentration increasing to 23.0% and 26.0% for the hydrogen and oxygen treated samples, respectively, seemingly due to the cleaning effect and removal of the adventitious carbon species present on the as-received sample. Interestingly, Figure 3b shows the valence band edge for the three samples with no significant change in the valence band onset ζ. Although the exact carrier concentration was not known for these samples it can be estimated by referring to similar work by Heinhold et al. that investigated Li concentration in ZnO crystals that had a resistivity as low as 0.3 Ohmcm, similar to the samples measured here.[53] The carrier concentration of the 0.3 Ohmcm crystals was ~1.1 x 10^{17} cm^{-3} (mobility ~190 cm^2/Vs) so we can estimate the as received sample with resistivity of ~0.5 ohmcm has a carrier concentration of ~6.6 x 10^{16} cm^{-3}.

The valence band offset (VBO) can be directly measured by collecting the photoelectrons emitted at energies from the Fermi level E_F to the valence band (VB) maximum E_V and beyond. The point at which the valence band emission onset occurs can be used to measure the VBO from the Fermi level and, with a well-defined bandgap the surface band bending can then be calculated in the following manner. A linear fit is extrapolated from the lower binding energy edge of the VB spectrum to a line fitted to the instrument background which provides the exact onset of the VB emission $\zeta=E_V-E_F$ as shown in Fig. 2b.[40,54] The position of the Fermi level E_F was calculated using the nanowire free carrier concentration *n* described above using $\xi = (kT/q)ln(N_C/n)$ relative to the conduction band (CB) minimum which gives ξ=0.0386 *eV*, where the CB effective density of states[44] for ZnO is $N_C=2.94x10^{18}\ cm^{-3}$. Therefore, the surface potential barrier V_{BB} can be calculated from measured ζ=3.41 *eV* as $V_{BB}=E_g-\xi-\zeta$, where $E_g=3.37\ eV$ is the bandgap of ZnO [20] which gives V_{BB} as approximately -0.08 *eV* ($\pm$0.05 *eV*). Positive values of V_{BB} correspond to upward band bending (and consequently surface electron depletion) while negative values indicate downward band bending (and electron accumulation) and a value of -0.08 *eV* indicates slight downward band bending at the surface compared to values between -0.2 to -0.4 *eV* that have previously been found on O-polar ZnO.[40]

It is possible that by using a conventional monochromated XPS with relatively high x-ray energies (i.e. electron inelastic mean free path of ~18 Å for *hv* = 1486.6 eV X-rays) that small changes in ζ were not detected and the higher energy x-rays were not surface sensitive enough to detect the light surface plasma treatments that were applied. Further investigation of this with lower photon energy synchrotron x-rays with a lower inelastic mean free path and increased surface sensitivity is required but for this study it shows that conventional or monochromated XPS, used for many studies of surfaces, in this instance cannot detect changes in surface band bending that are usually associated with changes in surface conductivity.[40,50,52,55] However, the effectiveness of the XPS analysis and the surface treatments is revealed by the O 1s peak and surface associated shoulder shown in Figure 3c.

Sample	Zn	O	C
As Received:	9.95 %	23.65 %	66.40 %
H plasma Treated:	23.01 %	39.97 %	37.02 %
O plasma Treated:	26.01 %	47.30 %	26.69 %

Table 1. Compositional XPS data for the as-received, hydrogen and oxygen plasma treated samples. A significant reduction in carbon is shown for both plasma treated samples and an increase in oxygen while the cleaning effect increases the Zn 2p 3/2 signal.

Examining the core-level peaks of O 1s and Zn 2p 3/2 we can infer some details of the surface chemistry that leads to the change in surface conductivity. Table 2 shows that there is no change to the Zn 2p 3/2 peak position confirming that no change in surface band bending occurred. Of most interest is the O 1s spectrum as this can reveal details of oxygen associated with hydroxyls, water, surface lattice oxygen and organic molecules. To examine the measured changes the O 1s peak was fitted with two or three Gaussian-Lorentzian components[53,56] which accurately matched the envelope to the raw data. The raw peaks are shown in Fig. 2c and the associated data in Table 2. To simplify the discussion we can label the main O 1s peak associated with the ZnO lattice as O- Zn, while the surface oxygen which occurs as a shoulder in the O 1s peak and at greater binding energy as O-S. The FWHM of the O-Zn component for each sample was fixed at 1.1 *eV* which was obtained from the fitting of the as-received sample O 1s data.

			Surface O		
	O 1s	Bulk O	$OH/O^{2-}/O_2^{2-}$	H_2O	Zn 2p 3/2
As-received	Peak (eV)	531.00	532.50	534.70	1022.40
	FWHM (eV)	1.10	2.00	2.00	1.80
	AT. %	46	48	6	-
H-plasma	Peak (eV)	531.00	532.50	n/a	1022.40
	FWHM (eV)	1.10	2.00	n/a	1.80
	AT. %	53	47	0	-
O-plasma	Peak (eV)	531.00	532.20	n/a	1022.40
	FWHM (eV)	1.10	2.00	n/a	1.80
	AT. %	42	58	0	-

Table 2. XPS Data for the three samples showing the binding energy peak positions for the O1s bulk peak and surface associated shoulder fitted with one or two Gaussian-Lorentzian components, the full width half maximum (FWHM) of each component, and the atomic percentage along with the same data for the Zn 2p 3/2 peak.

Both plasma treatments have had the effect of removing the H_2O component. The presence of undissociated water on the ZnO surface under the ultra-high vacuum conditions used in XPS has been previously reported by a number of authors and is attributed to extensive hydrogen bonding between adsorbed water molecules and the terminating hydroxyl groups on the ZnO surface that the plasma treatments disrupt.[44, 57, 58] For both the as-received and hydrogen (Figure 3c) treatments the proportion of the O-S component is similar, see Table 2, and the FWHM and binding energy remain the same. Most interestingly, the increase in oxygen content on the oxygen treated sample, see table 1, has had the effect of increasing the O-S atomic percentage to 58% when compared to the hydrogen treated sample that shows no increase in O-S from the as-received sample at 47%. The increase in O-S on the oxygen treated sample coincides with a shift in the O-S peak by 0.3 *eV* to a lower binding energy indicating that the chemical bonds of the surface oxygen are different between the two treatments. The interpretation of the O-S peak is inherently complex due to the variety of chemical interactions that oxygen and hydrogen can have with the ZnO surface. There are a number of plausible explanations for the O-S peak (often attributed to OH groups) being greater for the oxygen treated sample: (1) there could be a

different surface O contribution in addition to OH which is exhibited by the different O-S peak binding energy for the O-plasma treated sample that has shifted from the as-received and H-plasma treated samples; (2) the O-plasma treatment could increase the surface roughness and surface area which could increase the O-S signal (possibly revealing a greater contribution from H coming from the bulk of the ZnO crystal); (3) the O-plasma treatment removes/annihilates H_O defects (H multi-coordinated inside an oxygen vacancy) which are predicted to be shallow donors in ZnO increasing the sample resistivity.

The chemical interaction of hydrogen introduces OH groups to the surface increasing hydroxyl formation by reaction with lattice oxygen on the ZnO surface while also reacting with the adventitious carbon cleaning the surface. In comparison, oxygen plasma has the effect of reducing oxygen vacancies V_O and increasing Zn vacancies V_{Zn} in the ZnO lattice with oxygen radicals penetrating into the ZnO to form oxygen interstitials or antisite defects.[57,58] Hydrogen can induce surface metallicity[40,44,52,61,62] from binding of H to the lattice oxygen $O^{2-}+H\rightarrow OH^{-}+e^{-}$ where the hydroxyls act as donors.[45] This is enhanced by the reaction of hydrogen with adsorbed surface oxygen ions that act as acceptors (O^{-}, O^{2-}).[61] The oxygen plasma has the effect of reducing the number of oxygen vacancies and/or increasing Zn vacancies which reduce the carrier concentration near the surface increasing the sample resistivity as shown by the multi-probe transport measurements.[30,51,56,64,65]

The O-S peak of the as-received sample originates from a combination and balance of adsorbed surface oxygen ions, H_2O, hydroxyls and adventitious carbon/hydrocarbons molecules all competing for adsorption sites. The emission associated with hydroxyl groups, or O^{2-} ions in oxygen deficient regions on the ZnO surface, is often considered to be at a BE of $\sim$1 *eV* nearer to the O-Zn peak than adsorbed H_2O, O^{2-} and oxocarbons which are generally considered to create a peak at up to ~3 *eV* greater BE than the O-Zn.[44,55,66,67] The measurements in the case here show the O-S peak for the oxygen plasma treatment is closer in BE to the O-Zn peak than the as-received and hydrogen treated samples. The observed difference in O-S BE is not large enough to allow fitting of 2 separate O-S peaks which could be clearly labelled as hydroxyls and adsorbed oxygen for the H-plasma and O-plasma samples. This is because the peak separation of O-S to O-Zn (Table 2) for all samples is approximate to the separation of ~1.4 *eV* often attributed to hydroxyl bonds.[44,51]

However, the other evidence provided by the electrical measurements and the detailed data of the O1s shoulder show there are some significant differences between the samples that lower photon energy synchrotron x-rays with a lower inelastic mean free path and increased surface sensitivity could uncover.

The presence of the C-O bond from the solvent treatment on the as-received sample will likely have the effect of changing the O-S position to a different BE to that of hydroxyl bonds alone, to a similar position as the BE of 532.5 *eV* that has been attributed to adventitious CO_2 adsorbed to the ZnO surface.[68] Additionally, oxidising treatments can act to reduce oxygen point defects near the ZnO surface, which may increase the emission due to O^{2-}/O_2^{2-} that can appear at a similar BE as O-H bonds.[67] The oxidising effect of the plasma treatment provides the measured increase in O-S and consequent reduction in sample conductivity.[50] The valence band spectra, electrical measurements and the detailed data of the O1s shoulder show there are some significant differences between the samples that are only truly revealed by the multi-probe STM measurements. To explain the observed change in O–S BE for the hydrogen treated sample we can look at the reaction of H that will create a hydroxyl with a surface lattice O Atom. The resulting effect is for hydrogen to act as a reducing agent and donate electrons at the surface, hence, the relatively lower concentration of O shown in table 1 and vastly lower resistivity and prominent surface conductivity.

Conclusions

The multi-probe measurements have been shown to reveal changes in surface conductivity that cannot be directly correlated to surface band bending as studied using monochromated XPS. The treatment of the same $(000\bar{1})$ bulk ZnO single crystal with relatively moderate hydrogen and oxygen plasma provided a significant change in sample resistivity and revealed surface conduction that results from surface hydrogen doping. Significant correlation using XPS with changes in sample resistivity were only detectable by the analysis of the O1s and surface oxygen XPS components. These results have confirmed that multi-probe STM is a prime technique for detecting surface modifications that are beyond other staple surface science techniques.

Acknowledgements

AML would like to thank the support of the Sêr Cymru II fellowship scheme part-funded by the European Regional Development Fund through the Welsh Government and the facilities at the Centre for NanoHealth, Swansea University, UK. JEE would like to thank the Engineering Research Network Wales. MWA acknowledges support from the Royal Society of New Zealand Rutherford Discovery Fellowship scheme. CJB acknowledges the support from the Sêr Cyrmu NRN scheme. Support was provided to ARB by the Welsh Government Sêr Cymru Programme, through the Sêr Cymru Chair for Low Carbon Energy and Environment and the Robert A. Welch Foundation (C-0002). Support was provided by the Engineering and Physical Sciences Research Council-funded Impact Acceleration Account [grant number EP/K504002/1].

References

[1] Shiraki I, Nagao T, Hasegawa S, Petersen C L, Bøggild P, Hansen T M and Hansen F 2000 Micro-four-point probes in a uhv scanning electron microscope for in-situ surface-conductivity measurements *Surf. Rev. Lett.* **7** 533–7

[2] Shiraki I, Tanabe F, Hobara R, Nagao T and Hasegawa S 2001 Independently driven four-tip probes for conductivity measurements in ultrahigh vacuum *Surf. Sci.* **493** 633–43

[3] Hasegawa S, Shiraki I, Tanabe F, Hobara R, Kanagawa T, Tanikawa T, Matsuda I, Petersen C L, Hansen T M, Boggild P And Grey F 2003 Electrical conduction through surface superstructures measured by microscopic four-point probes *Surf. Rev. Lett.* **10** 963–80

[4] Bauer S, Bobisch C A, Klasing F, Hanisch-Blicharski A and Hoegen M H 2016 Nanoscale electron transport at the surface of a topological insulator *Nat. Commun.* **7** 11381

[5] Yang J, Sordes D, Kolmer M, Martrou D and Joachim C 2016 Imaging, single atom contact and single atom manipulations at low temperature using the new ScientaOmicron LT-UHV-4 STM *Eur. Phys. J. Appl. Phys.* **73** 10702

[6] Edler F, Miccoli I, Stöckmann J P, Pfnür H, Braun C, Neufeld S, Sanna S, Schmidt W G

and Tegenkamp C 2017 Tuning the conductivity along atomic chains by selective chemisorption *Phys. Rev. B* **95** 125409

[7] Song F, Wells J W, Handrup K, Li Z S, Bao S N, Schulte K, Ahola-Tuomi M, Mayor L C, Swarbrick J C, Perkins E W, Gammelgaard L and Hofmann P 2009 Direct measurement of electrical conductance through a self-assembled molecular layer *Nat. Nanotechnol.* **4** 373–6

[8] Ma Y, Kolekar S, Coy Diaz H, Aprojanz J, Miccoli I, Tegenkamp C and Batzill M 2017 Metallic Twin Grain Boundaries Embedded in MoSe 2 Monolayers Grown by Molecular Beam Epitaxy *ACS Nano* acsnano.7b02172

[9] Lord A M, Maffeis T G, Kryvchenkova O, Cobley R J, Kalna K, Kepaptsoglou D M D, Ramasse Q M, Walton A S, Ward M B, Koeble J and Wilks S P 2015 Controlling the electrical transport properties of nanocontacts to nanowires. *Nano Lett.* **15** 4248–54

[10] Lord A M, Maffeis T G, Walton A S, Kepaptsoglou D M, Ramasse Q M, Ward M B, Köble J and Wilks S P 2013 Factors that determine and limit the resistivity of high-quality individual ZnO nanowires. *Nanotechnology* **24** 435706

[11] Lord A M, Ramasse Q M, Kepaptsoglou D M, Evans J E, Davies P R, Ward M B and Wilks S P 2017 Modifying the Interface Edge to Control the Electrical Transport Properties of Nanocontacts to Nanowires *Nano Lett.* **17** 687–94

[12] Walton A S, Allen C S, Critchley K, Górzny M Ł, McKendry J E, Brydson R M D, Hickey B J and Evans S D 2007 Four-probe electrical transport measurements on individual metallic nanowires *Nanotechnology* **18** 65204

[13] Korte S, Steidl M, Prost W, Cherepanov V, Voigtländer B, Zhao W, Kleinschmidt P and Hannappel T 2013 Resistance and dopant profiling along freestanding GaAs nanowires *Appl. Phys. Lett.* **103** 143104

[14] Just S, Soltner H, Korte S, Cherepanov V and Voigtländer B 2017 Surface conductivity of Si(100) and Ge(100) surfaces determined from four-point transport measurements using an analytical N -layer conductance model *Phys. Rev. B* **95** 075310

[15] Just S, Blab M, Korte S, Cherepanov V, Soltner H and Voigtländer B 2015 Surface and Step Conductivities on Si(111) Surfaces *Phys. Rev. Lett.* **115** 66801

[16] Choi K J and Jang H W 2010 One-dimensional oxide nanostructures as gas-sensing materials: Review and issues *Sensors* **10** 4083–99

[17] Mikkelsen A and Lundgren E 2013 Surface science of free standing semiconductor nanowires *Surf. Sci.* **607** 97–105

[18] Wells J W, Kallehauge J F and Hofmann P 2008 Surface-sensitive conductance measurements on clean and stepped semiconductor surfaces: Numerical simulations of four point probe measurements *Surf. Sci.* **602** 1742–9

[19] Hofmann P and Wells J W 2009 Surface-sensitive conductance measurements *J. Phys. Condens. Matter* **21** 13003

[20] Li P-J, Liao Z-M, Zhang X-Z, Zhang X-J, Zhu H-C, Gao J-Y, Laurent K, Leprince-Wang Y, Wang N and Yu D-P 2009 Electrical and Photoresponse Properties of an Intramolecular p-n Homojunction in Single Phosphorus-Doped ZnO Nanowires *Nano Lett.* **9** 2513–8

[21] Jacobs K, Balitsky D, Armand P and Papet P 2010 Low-temperature chemical bath deposition of crystalline ZnO *Solid State Sci.* **12** 333–8

[22] Tarat A, Nettle C J, Bryant D T J, Jones D R, Penny M W, Brown R A, Majitha R, Meissner K E and Maffeis T G G 2014 Microwave-assisted synthesis of layered basic zinc acetate nanosheets and their thermal decomposition into nanocrystalline ZnO *Nanoscale Res. Lett.* **9** 11

[23] Yang P, Yan H, Mao S, Russo R, Johnson J, Saykally R, Morris N, Pham J, He R and Choi H-J 2002 Controlled Growth of ZnO Nanowires and Their Optical Properties *Adv. Funct. Mater.* **12** 323–31

[24] Dulub O, Boatner L A and Diebold U 2002 STM study of the geometric and electronic structure of ZnO(0001)-Zn, (000-1 1 1)-O, (10-1 10), and (11-2 20) surfaces *Surf. Sci.* **519** 201–17

[25] Kresse G, Dulub O and Diebold U 2003 Competing stabilization mechanism for the polar ZnO(0001)-Zn surface *Phys. Rev. B* **68** 245409

[26] Önsten A, Stoltz D, Palmgren P, Yu S, Göthelid M and Karlsson U O 2010 Water Adsorption on ZnO(0001): Transition from Triangular Surface Structures to a Disordered Hydroxyl Terminated phase *J. Phys. Chem. C* **114** 11157–61

[27] Valtiner M, Borodin S and Grundmeier G 2008 Stabilization and Acidic Dissolution Mechanism of Single-Crystalline ZnO(0001) Surfaces in Electrolytes Studied by In-Situ AFM Imaging and Ex-Situ LEED *Langmuir* **24** 5350–8

[28] Kunat M, Gil Girol S, Becker T, Burghaus U and Wöll C 2002 Stability of the polar surfaces of ZnO: A reinvestigation using He-atom scattering *Phys. Rev. B* **66** 81402

[29] Meyer B 2004 First-principles study of the polar O-terminated ZnO surface in thermodynamic equilibrium with oxygen and hydrogen *Phys. Rev. B* **69** 45416

[30] Brillson L J, Mosbacker H L, Hetzer M J, Strzhemechny Y, Jessen G H, Look D C, Cantwell G, Zhang J and Song J J 2007 Dominant effect of near-interface native point defects on ZnO Schottky barriers *Appl. Phys. Lett.* **90** 102116

[31] Tumakha S, Ewing D J, Porter L M, Wahab Q, Ma X, Sudharshan T S and Brillson L J 2005 Defect-driven inhomogeneities in Ni⁄4H–SiC Schottky barriers *Appl. Phys. Lett.* **87** 242106

[32] Ibe J P, Bey P P, Brandow S L, Brizzolara R A, Burnham N A, DiLella D P, Lee K P, Marrian C R K and Colton R J 1990 On the electrochemical etching of tips for scanning tunneling microscopy *J. Vac. Sci. Technol. A Vacuum, Surfaces, Film.* **8** 3570–5

[33] Cobley R J, Brown R a., Barnett C J, Maffeis T G G and Penny M W 2013 Quantitative analysis of annealed scanning probe tips using energy dispersive x-ray spectroscopy *Appl. Phys. Lett.* **102** 23111

[34] Barnett C J, Kryvchenkova O, Wilson L S J, Maffeis T G G, Kalna K and Cobley R J 2015 The role of probe oxide in local surface conductivity measurements *J. Appl. Phys.* **117** 174306

[35] Smith N A, Lord A M, Evans J E, Barnett C J, Cobley R J and Wilks S P 2015 Forming reproducible non-lithographic nanocontacts to assess the effect of contact compressive strain in nanomaterials *Semicond. Sci. Technol.* **30** 65011

[36] Lord A M, Walton A S, Maffeis T G, Ward M B, Davies P and Wilks S P 2014 ZnO Nanowires with Au Contacts Characterised in the as-grown Real Device configuration using a Local Multi-Probe Method *Nanotechnology* **25** 425706

[37] Lord A M, Ward M B, Evans J E, Davies P R, Smith N A, Maffeis T G and Wilks S P 2014 Enhanced Long-Path Electrical Conduction in ZnO Nanowire Array Devices Grown via Defect-Driven Nucleation *J. Phys. Chem. C* **118** 21177–21184

[38] Miccoli I, Edler F, Pfnür H and Tegenkamp C 2015 The 100th anniversary of the four-point probe technique: the role of probe geometries in isotropic and anisotropic systems *J. Phys. Condens. Matter* **27** 223201

[39] Valdes L B 1954 Resistivity Measurements on Germanium for Transistors *Proc. IRE* **42** 420–7

[40] Allen M W, Swartz C H, Myers T H, Veal T D, McConville C F and Durbin S M 2010 Bulk transport measurements in ZnO: The effect of surface electron layers *Phys. Rev. B* **81** 75211

[41] Van de Walle C G 2000 Hydrogen as a Cause of Doping in Zinc Oxide *Phys. Rev. Lett.* **85** 1012–5

[42] Janotti A and Van de Walle C G 2007 Hydrogen multicentre bonds *Nat. Mater.* **6** 44–7

[43] Brillson L J, Ruane W T, Gao H, Zhang Y, Luo J, von Wenckstern H and Grundmann M 2017 Spatially-resolved cathodoluminescence spectroscopy of ZnO defects *Mater. Sci. Semicond. Process.* **57** 197–209

[44] Heinhold R, Williams G T, Cooil S P, Evans D A and Allen M W 2013 Influence of polarity and hydroxyl termination on the band bending at ZnO surfaces *Phys. Rev. B* **88** 235315

[45] Janotti A and Van de Walle C G 2009 Fundamentals of zinc oxide as a semiconductor

Reports Prog. Phys. **72** 126501

[46] Schmidt O, Geis A, Kiesel P, Van de Walle C G, Johnson N M, Bakin A, Waag A and Döhler G H 2006 Analysis of a conducting channel at the native zinc oxide surface *Superlattices Microstruct.* **39** 8–16

[47] Coppa B J, Davis R F and Nemanich R J 2003 Gold Schottky contacts on oxygen plasma-treated, *n* -type ZnO(000$\bar{1}$) *Appl. Phys. Lett.* **82** 400–2

[48] Strzhemechny Y M, Mosbacker H L, Look D C, Reynolds D C, Litton C W, Garces N Y, Giles N C, Halliburton L E, Niki S and Brillson L J 2004 Remote hydrogen plasma doping of single crystal ZnO *Appl. Phys. Lett.* **84** 2545–7

[49] Sekiguchi T, Ohashi N and Terada Y 1997 Effect of Hydrogenation on ZnO Luminescence *Jpn. J. Appl. Phys.* **36** L289–91

[50] Lord A M, Maffeis T G, Allen M W, Morgan D, Davies P R, Jones D R, Evans J E, Smith N A and Wilks S P 2014 Surface state modulation through wet chemical treatment as a route to controlling the electrical properties of ZnO nanowire arrays investigated with XPS *Appl. Surf. Sci.* **320** 664–9

[51] Heinhold R and Allen M W 2012 Polarity-dependent photoemission of in situ cleaved zinc oxide single crystals *J. Mater. Res.* **27** 2214–9

[52] Heinhold R, Cooil S P, Evans D A and Allen M W 2014 Stability of the Surface Electron Accumulation Layers on the Non-polar (10$\bar{1}$0) and (11$\bar{2}$0) Faces of ZnO *J. Phys. Chem. C* **118** 24575–82

[53] Heinhold R, Kim H-S, Schmidt F, von Wenckstern H, Grundmann M, Mendelsberg R J, Reeves R J, Durbin S M and Allen M W 2012 Optical and defect properties of hydrothermal ZnO with low lithium contamination *Appl. Phys. Lett.* **101** 62105

[54] Lyons J L, Janotti A and Walle C G Van de 2009 Why nitrogen cannot lead to p-type conductivity in ZnO *Appl. Phys. Lett.* **95** 252105

[55] Maffeis T G G, Penny M W, Castaing A, Guy O J and Wilks S P 2012 XPS investigation of vacuum annealed vertically aligned ultralong ZnO nanowires *Surf. Sci.* **606** 99–103

[56] Hu Y, Liu Y, Xu H, Liang X, Peng L-M, Lam N, Wong K and Li Q 2008 Quantitative Study on the Effect of Surface Treatments on the Electric Characteristics of ZnO Nanowires *J. Phys. Chem. C* **112** 14225–8

[57] Meyer B, Marx D, Dulub O, Diebold U, Kunat M, Langenberg D and Wöll C 2004 Partial Dissociation of Water Leads to Stable Superstructures on the Surface of Zinc Oxide Angew. Chem., Int. Ed. **43** 6642−6645

[58] Raymand D, van Duin A C T, Goddard W A, Hermansson K and Spangberg D 2011, Hydroxylation Structure and Proton Transfer Reactivity at the Zinc Oxide−Water Interface J. Phys. Chem. C **115** 8573−8579

[59] Tsai C-H, Wang W-C, Jenq F-L, Liu C-C, Hung C-I and Houng M-P 2008 Surface modification of ZnO film by hydrogen peroxide solution *J. Appl. Phys.* **104** 53521

[60] Gu Q L, Ling C C, Chen X D, Cheng C K, Ng A M C, Beling C D, Fung S, Djurišić A B, Lu L W, Brauer G and Ong H C 2007 Hydrogen peroxide treatment induced rectifying behavior of Au/n-ZnO contact *Appl. Phys. Lett.* **90** 122101

[61] Mendelsberg R J, Allen M W, Durbin S M and Reeves R J 2011 Photoluminescence and the exciton-phonon coupling in hydrothermally grown ZnO *Phys. Rev. B* **83** 205202

[62] Lavrov E V., Weber J, Börrnert F, Van de Walle C G and Helbig R 2002 Hydrogen-related defects in ZnO studied by infrared absorption spectroscopy *Phys. Rev. B* **66** 165205

[63] Coppa B J, Fulton C C, Kiesel S M, Davis R F, Pandarinath C, Burnette J E, Nemanich R J and Smith D J 2005 Structural, microstructural, and electrical properties of gold films and Schottky contacts on remote plasma-cleaned, n-type ZnO{0001} surfaces *J. Appl. Phys.* **97** 103517

[64] Gu Q L, Cheung C K, Ling C C, Ng A M C, Djurišić A B, Lu L W, Chen X D, Fung S, Beling C D and Ong H C 2008 Au/n-ZnO rectifying contact fabricated with hydrogen peroxide pretreatment *J. Appl. Phys.* **103** 93706

[65] Schifano R, Monakhov E V., Svensson B G and Diplas S 2009 Surface passivation and interface reactions induced by hydrogen peroxide treatment of n-type ZnO (0001) *Appl. Phys. Lett.* **94** 132101

[66] Park S-M, Ikegami T and Ebihara K 2006 Effects of substrate temperature on the properties of Ga-doped ZnO by pulsed laser deposition *Thin Solid Films* **513** 90–4

[67] Tam K H, Cheung C K, Leung Y H, Djurisić A B, Ling C C, Beling C D, Fung S, Kwok W M, Chan W K, Phillips D L, Ding L and Ge W K 2006 Defects in ZnO nanorods prepared by a hydrothermal method. *J. Phys. Chem. B* **110** 20865–71

[68] Lupan O, Emelchenko G A, Ursaki V V, Chai G, Redkin A N, Gruzintsev A N, Tiginyanu I M, Chow L, Ono L K, Roldan Cuenya B, Heinrich H and Yakimov E E 2010 Synthesis and characterization of ZnO nanowires for nanosensor applications *Mater. Res. Bull.* **45** 1026–32

[69] Lee H-Y, Wu B-K and Chern M-Y 2014 Study on the formation of zinc peroxide on zinc oxide with hydrogen peroxide treatment using x-ray photoelectron spectroscopy (XPS) *Electron. Mater. Lett.* **10** 51–5